Journal of Materials and Environmental Science
ISSN : 2028-2508
e-ISSN : 2737-890X
CODEN : JMESCN

J. Mater. Environ. Sci., 2023, Volume 14, Issue 05, Page 520-538

http://www.jmaterenvironsci.com

Variation Iteration Method to the Investigations of Surface Energy, Initial Stress and Nonlocality on Vibration of Carbon Nanotubes Conveying Fluid Resting on Elastic Foundations in a Thermo-Magnetic Environment

Temitayo I. Olaleye[1], Suraju A. Oladosu[2], Rafiu O. Kuku[3], Gbeminiyi M. Sobamowo[4]

[1,2,3]*Department of Mechanical Engineering, Faculty of Engineering, Lagos State University, Epe Campus, Lagos. Nigeria*
[43]*Department of Mechanical Engineering, Faculty of Engineering, University of Lagos, Akoka, Yaba, Lagos. Nigeria.*

[4]*Corresponding author, Email address: gsobamowo@unilag.edu.ng*

Received *15 March 2023,*
Revised *26 Apr 2023,*
Accepted *01 May 2023*

Keywords:
- ✓ Surface Effects
- ✓ Carbon nanotubes;
- ✓ Nonlocal elasticity theory
- ✓ Variational Iteration method

Citation: *Olaleye T. A., Oladosu S. A., Kuku R. O. Sobamowo, M. G. (2023) Variation Iteration Method for the Investigations of Surface Energy, Initial Stress and Nonlocality on Vibration of Carbon Nanotubes Conveying Fluid Resting on Elastic Foundations in a Thermo-Magnetic Environment J. Mater. Environ. Sci., 14(5), 520-538.*

Abstract: This work applies variation iteration method to study the simultaneous impacts of surface elasticity, initial stress, residual surface tension and nonlocality on the nonlinear vibration of single-walled carbon conveying nanotube resting on linear and nonlinear elastic foundation and operating in a thermo-magnetic environment. Equation of motion governing the vibration of the nanotube was derived using Erigen's theory, Euler-Bernoulli's theory and Hamilton's principle. The partial differential equation was converted to ordinary differential equation using Galerkin's decomposition method and the ordinary differential equation was solved with the aid of variational of iteration method. Through the parametric studies, it was revealed that the ratio of the nonlinear to linear frequencies increases with the negative value of the surface stress while it decreases with the positive value of the surface stress. At any given value of nonlocal parameters, the surface effect reduces for increasing in the length of the nanotube. ratio of the frequencies decreases with increase in the strength of the magnetic field, nonlocal parameter and the length of the nanotube. The natural frequency of the nanotube gradually approaches the nonlinear Euler–Bernoulli beam limit at high values of nonlocal parameter and nanotube length. nonlocal parameter reduces the surface effects on the ratio of the frequencies. Increase in temperature change at high temperature causes decrease in the frequency ratio. However, at room or low temperature, the frequency ratio of the hybrid nanostructure increases as the temperature change increases. Also, the ratio of the frequencies at low temperatures is lower than at high temperatures. The present work will assist in the control and design of carbon nanotubes operating in thermo-magnetic environment and resting on elastic foundations.

1. Introduction

After the discovery of nanostructures discovered by Iijima (1991), different studies on the utilizations of nanomaterials have showed the importance of carbon nanotubes (CNTs) for medical, industrial, electrical, thermal, electronic and mechanical applications (Abgrall and Nguyen(2008), Zhao et al. (2018), A. Azrar et al. (2018), Rashidi et al. (2012)). The previous works on the vibrations analysis of nanotubes show some novel developments in the dynamic characterization of the nanostructures, with continuous and recent developments in nano-materials research (Reddy and Pang (2008), Wang (2011), Lim (2010), Lim and Yang (2010), Bahaadini and Hosseini (2016), Mahinzare et al. (2017), Bahaadini and Hosseini (2018) and Wang (2010)). However, the effects of the surface energy and initial stress are neglected in the studies. Indisputably, the properties of the region of the solid surface are different properties from the bulk material. Also, for classical structures, surface energy-to-bulk energy ratio is small. However, nanostructures have large surface energy-to-bulk energy ratio and high ratio of surface energies to volume, elastic modulus and mechanical strength. Consequently, the mechanical behaviours, bending deformation and elastic waves of the nanostructures are greatly influenced. Therefore, the surface energy effects cannot be neglected in the dynamic behaviour analysis of nanostructures. Such surface energy of nanostructures is composed of the surface tension and surface modulus exerted on the surface layer of nanostructures (Zhang and Meguid (2016), Hosseini et al. (2016), Bahaadini et al. (2017), Wang and Feng (2007, 2009), Farshi et al. (2010), Lee and Chang (2011)). Using nonlocal elasticity theory, Wang (2010) analyzed surface effects on the vibration behaviour of carbon nanotubes. Few years later, Zhang and Meguid (2016) presented the impacts of surface energy on the dynamic behaviour and instability of nanobeams conveying fluids. Hosseini et al. (2016) studied the influence of surface energy on the nonlocal instability of cantilever piezoelectric carbon nanotubes conveying fluid. The combined effects of surface energy and nonlocality on the flutter instability of cantilevered nanotubes conveying fluid under the influence of follower forces were explored by Bahaadini et al. (2017). Using nonlocal elasticity theory, Wang and Feng (2007, 2009) investigated the effects of the surface stress on contact problems at nanoscale and proposed a theoretical model considering the joint effects of the elastic modulus of the surface and residual stress for vibration analysis on the basis of Euler-Bernoulli beam model. Lee and Chang (2010, 2011) confirmed the surface effect plays a significant role on vibration frequency of nano-beam through the Rayleigh-Ritz method. Other researchers (Guo and Zhao (2007), Feng et al. (2009), He et al. (2008a, 2008b), Jing et al. (2006), Sharm et al. (2003), Wang et al. (2010)) also examined the significance of surface stress and energy on the dynamic response and instability of nanostructures.

Carbon nanotubes often suffer from initial stresses due to residual stress, thermal effects, surface effects, mismatches between the material properties of CNTs and surrounding mediums, initial external loads and other physical issues. The effects of initial stress on the dynamic behaviour of nanotubes have been studied (Selim (2009), Zhang and Wang (2006), Wang and Cai (2006), Sun and Liu (2007), Chen and Wang (2008), Selim (2010, 2011a, 2011b), Selim and El-Safty (2020). However, because of their significant in practically nano-apparatus applications, there is a need for a combined on the effects of surface behaviours, initial stress and nonlocality on the physical characteristics and mechanical behaviours of carbon nanotubes. Also, scanning through the past works and to the best of the authors' knowledge, a study on simultaneous effects of surface energy and initial stress on the vibration characteristics of nanotubes resting of Winkler and Pasternak foundations in a thermo-magnetic environment has not been carried out. Therefore, in this present study, the coupled impacts of surface effects, initial stress and nonlocality on the nonlinear dynamic behaviour of single-walled carbon nanotubes resting on Winkler (Spring) and Pasternak (Shear layer) foundations in a thermal-magnetic environment. Erigen's nonlocal elasticity (1972a, 1972b, 1983), Maxwell's relations, Hamilton's principle, surface effect and Euler-Bernoulli beam theories are adopted to develop the systems of nonlinear equations of the dynamics behaviour of the carbon nanotube. The partial differential equation was converted to ordinary differential equation using Galerkin's decomposition method and the ordinary differential equation was solved with the aid of variational of iteration method. Although, the study is majorly directed to analyze the impacts of surface, nonlocality and initial stress on the vibration of the nanostructures, it is known that magnetic field and temperature change/gradients can significantly change the vibration characteristics of nanotubes as they affect the homogeneous nanotubes.

2. Model Development

Consider a single-walled CNT of length L and inner and outer diameters D_i and D_o resting on Winkler (Spring) and Pasternak (Shear layer) foundations as illustrated in Fig. 1. The SWCNTs conveying a hot fluid and resting on elastic foundation under external applied tension, initial stress, magnetic and temperature fields as shown in the figure.

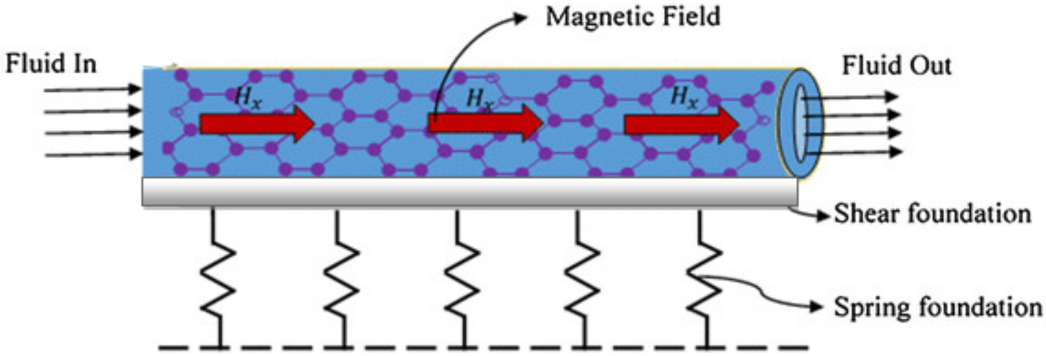

Fig. 1 Carbon nanotube conveying hot fluid resting on elastic foundation

2.3 Nonlocal elasticity theory

Based on the nonlocal elasticity theory and given considerations to the nonlocal effects of higher-order strain gradients, the differential relations involving the stress resultants and the strains for the nanotube:

$$\sigma_{xx} - (e_0 a)^2 \frac{\partial^2 \sigma_{xx}}{\partial x^2} = E\varepsilon_{xx} \tag{1}$$

The strain–displacement relation,

$$\varepsilon_{xx} = -z\frac{\partial^2 w(x,t)}{\partial x^2} \tag{2}$$

In case of small deformation, the strain strain–displacement relation

$$\varepsilon_{xx} = -z\frac{\partial^2 w}{\partial x^2} \tag{3}$$

Therefore,

$$\sigma_{xx} - (e_0 a)^2 \frac{\partial^2 \sigma_{xx}}{\partial x^2} = -Ez\frac{\partial^2 w}{\partial x^2} \tag{4}$$

Multiply Eq. (4) through by zdA

$$\sigma_{xx} zdA - (e_0 a)^2 \frac{\partial^2 (z\sigma_{xx})}{\partial x^2} dA = -Ez^2 \frac{\partial^2 w}{\partial x^2} dA \tag{5}$$

On integrating both sides of Eq. (8), we have

$$\int_A \sigma_{xx} zdA - (e_0 a)^2 \frac{\partial^2}{\partial x^2} \int_A z\sigma_{xx} dA = -E\frac{\partial^2 w}{\partial x^2} \int_A z^2 dA \tag{6}$$

Recall that the bending moment and second moment of area of the nanotube are given as

$$M = \int_A z\sigma_{xx} dA \tag{7}$$

and

$$I = \int_A z^2 dA \tag{8}$$

Therefore, Eq. (6) can be written as

$$M-\left(e_0a\right)^2\frac{\partial^2 M}{\partial x^2}=-EI\frac{\partial^2 w}{\partial x^2} \tag{9}$$

The above Eq. (9) shows the relationship between the flexural displacement w and the bending moment M of the nanotube can be obtained.

If Eq. (9) is differentiated twice, we have

$$\frac{\partial^2 M}{\partial x^2}-\left(e_0a\right)^2\frac{\partial^2}{\partial x^2}\left(\frac{\partial^2 M}{\partial x^2}\right)=-EI\frac{\partial^4 w}{\partial x^4} \tag{10}$$

Therefore,

$$EI\frac{\partial^4 w}{\partial x^4}+\frac{\partial^2 M}{\partial x^2}-\left(e_0a\right)^2\frac{\partial^2}{\partial x^2}\left(\frac{\partial^2 M}{\partial x^2}\right)=0 \tag{11}$$

If the effect of surface is considered, we have

$$\left(EI+E_sI_s\right)\frac{\partial^4 w}{\partial x^4}+\frac{\partial^2 M}{\partial x^2}-\left(e_0a\right)^2\frac{\partial^2}{\partial x^2}\left(\frac{\partial^2 M}{\partial x^2}\right)=0 \tag{12}$$

From the Euler beam theory,

$$\frac{\partial^2 M}{\partial x^2}=m_{cn}\frac{\partial^2 w}{\partial t^2}+f_{fluid\ flow}-f_{initial\,stress}+f_{axial\,tension}+f_{residual\ surface\,stress}+f_{foundation}+f_{magnetic}-f_{thermal} \tag{13}$$

The axial force per unit length as a result fluid flow effect

$$f_{fluid\ flow}=m_f\frac{\partial^2 w}{\partial t^2}+m_fu^2\frac{\partial^2 w}{\partial x\partial t}+2um_f\frac{\partial^2 w}{\partial x\partial t} \tag{14}$$

The axial force per unit length due to initial stress

$$f_{initial\,stress}=-\delta A\sigma_x^o\frac{\partial^2 w}{\partial x^2} \tag{15}$$

The axial force per unit length due to residual surface stress

$$f_{residual\ surface\,stress}=H_s\frac{\partial^2 w}{\partial x^2} \tag{16}$$

The axial force per unit length due to axial tension/support

$$f_{axial\,\mathrm{support}}=\left[\frac{EA}{2L}\int_0^L\left(\frac{\partial w}{\partial x}\right)^2dx\right]\frac{\partial^2 w}{\partial x^2} \tag{17}$$

The force per unit length due to the Winkler and Pasternak foundations is given as

$$f_{foundation}=k_1w-k_p\frac{\partial^2 w}{\partial x^2}+k_3w^3 \tag{18}$$

The magnetic force per unit length as a result of Lorentz force.

$$f_{magnetic}=\eta H_x^2A\frac{\partial^2 w}{\partial x^2} \tag{19}$$

The axial force per unit length as a result of the thermal effect

$$f_{thermal}=-\frac{EA\alpha\Delta T}{1-2\nu}\frac{\partial^2 w}{\partial x^2} \tag{20}$$

Substituting Eqs. (14) – (20) into Eq. (13), we have

$$\frac{\partial^2 M}{\partial x^2} = (m_{cn} + m_f)\frac{\partial^2 w}{\partial t^2} + 2um_f\frac{\partial^2 w}{\partial x \partial t} + \left[\frac{EA}{2L}\int_0^L \left(\frac{\partial w}{\partial x}\right)^2 dx\right]\frac{\partial^2 w}{\partial x^2} + \left(m_f u^2 + \delta A\sigma_x^o - H_s - \eta H_x^2 A - k_p + \frac{EA\alpha\Delta T}{1-2\nu}\right)\frac{\partial^2 w}{\partial x^2} + k_1 w + k_3 w^3 \tag{21}$$

On putting Eq. (20) into Eq. (12), we arrived at

$$\begin{aligned}&\left(EI + E_s I_s\right)\frac{\partial^4 w}{\partial x^4} + (m_{cn} + m_f)\frac{\partial^2 w}{\partial t^2} + 2um_f\frac{\partial^2 w}{\partial x \partial t} + \left[\frac{EA}{2L}\int_0^L \left(\frac{\partial w}{\partial x}\right)^2 dx\right]\frac{\partial^2 w}{\partial x^2}\\ &+\left(m_f u^2 + \delta A\sigma_x^o - H_s - \eta H_x^2 A - k_p + \frac{EA\alpha\Delta T}{1-2\nu}\right)\frac{\partial^2 w}{\partial x^2} + k_1 w + k_3 w^3\\ &-\left(e_o a\right)^2\left[\begin{aligned}&(m_{cn} + m_f)\frac{\partial^4 w}{\partial x^2 \partial t^2} + 2um_f\frac{\partial^4 w}{\partial x^3 \partial t} + \left[\frac{EA}{2L}\int_0^L \left(\frac{\partial w}{\partial x}\right)^2 dx\right]\frac{\partial^4 w}{\partial x^4}\\ &+\left(m_f u^2 + \delta A\sigma_x^o - H_s - \eta H_x^2 A - k_p + \frac{EA\alpha\Delta T}{1-2\nu}\right)\frac{\partial^4 w}{\partial x^4}\\ &+k_1\frac{\partial^2 w}{\partial x^2} + 3k_3 w^2\frac{\partial^2 w}{\partial x^2} + 6k_3 w\left(\frac{\partial w}{\partial x}\right)^2\end{aligned}\right] = 0\end{aligned} \tag{22}$$

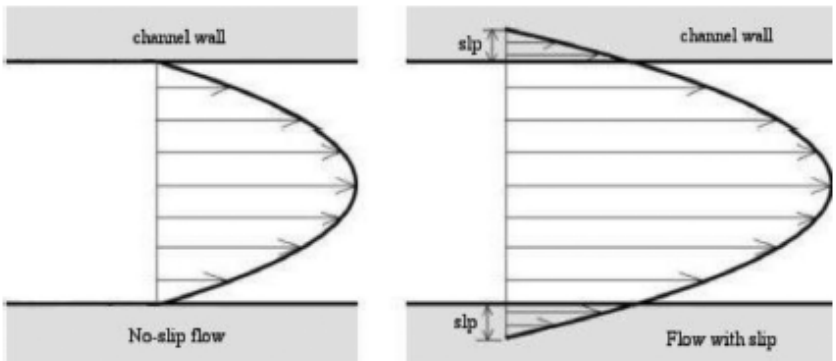

Fig. 2. Effect of slip boundary condition on velocity profile Arania et al. (2016), Bahaadini and Hosseini (2016)

Fig. 2 shows the effect of flow in a channel. In the fluid-conveying carbon nanotube, the condition of slip is satisfied since in such flow, the ratio of the mean free path of the fluid molecules relative to a characteristic length of the flow geometry which is the Knudsen number is larger than 10^{-2}. Consequently, the velocity correction factor for the slip flow velocity is proposed by Arania et al. (2016), Bahaadini and Hosseini (2016) as

$$VCF = \frac{u_{avg,slip}}{u_{avg,no-slip}} = \left(1 + a_k Kn\right)\left[4\left(\frac{2-\sigma_v}{\sigma_v}\right)\left(\frac{Kn}{1+Kn}\right) + 1\right] \tag{23}$$

Where Kn is the Knudsen number, σ_v is tangential moment accommodation coefficient which is considered to be 0.7 for most practical purposes (Arania et al. (2016), Bahaadini and Hosseini (2016)):

$$a_k = a_o\frac{2}{\pi}\left[tan^{-1}\left(a_1 Kn^B\right)\right] \tag{24}$$

$$a_o = \frac{64}{3\pi\left(1 - \frac{4}{b}\right)} \tag{25}$$

$a_1 = 4$ and B = 0.04 and b is the general slip coefficient ($b = -1$).

From Eq. (23),

$$u_{avg,slip} = \left(1 + a_k Kn\right)\left[4\left(\frac{2-\sigma_v}{\sigma_v}\right)\left(\frac{Kn}{1+Kn}\right)+1\right]u_{avg,no-slip} \tag{26}$$

Therefore, Eq. (22) can be written as

$$\begin{gathered}\left(EI + E_s I_s\right)\frac{\partial^4 w}{\partial x^4} + (m_{cn} + m_f)\frac{\partial^2 w}{\partial t^2} + 2m_f\left(1 + a_k Kn\right)\left[4\left(\frac{2-\sigma_v}{\sigma_v}\right)\left(\frac{Kn}{1+Kn}\right)+1\right]\frac{\partial^2 w}{\partial x \partial t} + \left[\frac{EA}{2L}\int_0^L\left(\frac{\partial w}{\partial x}\right)^2 dx\right]\frac{\partial^2 w}{\partial x^2} \\ + \left(m_f\left[\left(1 + a_k Kn\right)\left[4\left(\frac{2-\sigma_v}{\sigma_v}\right)\left(\frac{Kn}{1+Kn}\right)+1\right]\right]^2 + \delta A\sigma_x^o - H_s - \eta H_x^2 A - k_p + \frac{EA\alpha\Delta T}{1-2\nu}\right)\frac{\partial^2 w}{\partial x^2} + k_1 w + k_3 w^3 \\ -\left(e_o a\right)^2\left[\begin{array}{l}(m_{cn} + m_f)\dfrac{\partial^4 w}{\partial x^2 \partial t^2} + 2m_f\left(1 + a_k Kn\right)\left[4\left(\dfrac{2-\sigma_v}{\sigma_v}\right)\left(\dfrac{Kn}{1+Kn}\right)+1\right]\dfrac{\partial^4 w}{\partial x^3 \partial t} + \left[\dfrac{EA}{2L}\displaystyle\int_0^L\left(\dfrac{\partial w}{\partial x}\right)^2 dx\right]\dfrac{\partial^4 w}{\partial x^4} \\ + \left(m_f\left[\left(1 + a_k Kn\right)\left[4\left(\dfrac{2-\sigma_v}{\sigma_v}\right)\left(\dfrac{Kn}{1+Kn}\right)+1\right]\right]^2 + \delta A\sigma_x^o - H_s - \eta H_x^2 A - k_p + \dfrac{EA\alpha\Delta T}{1-2\nu}\right)\dfrac{\partial^4 w}{\partial x^4} \\ + k_1\dfrac{\partial^2 w}{\partial x^2} + 3k_3 w^2\dfrac{\partial^2 w}{\partial x^2} + 6k_3 w\left(\dfrac{\partial w}{\partial x}\right)^2\end{array}\right] = 0\end{gathered} \tag{27}$$

where the transverse area and the bending rigidity are given as

$$A = \pi d h$$

$$EI = \frac{\pi d^3 h}{8}$$

and

$$E_s I_s = \frac{\pi E_s h(d_o^3 + d_i^3)}{8}$$

$$H_s = 2\tau_s\left(d_o + d_i\right)$$

The symbol H_s is the parameter induced by the residual surface stress**.** τ is the residual surface tension, d and h are the nanotube internal diameter and thickness, respectively. It should be noted that the diameter of the nanotube can be derived from chirality indices (n, m)

$$d_i = \frac{a\sqrt{3}}{\pi}\sqrt{n^2 + mn + m^2} \tag{28}$$

where $a\sqrt{3} = 0.246\,nm$. ”a” represents the length of the carbon-carbon bond. d is the inner diameter of the nanotube.

3. Analytical Solutions of Nonlinear Model of Free Vibration of the nanotube

The nonlinear term in model in Eq. (27) makes it very difficult to provide closed-form solution to the problem. Therefore, recourse is made to homotopy perturbation to solve the nonlinear model. In order to develop analytical solutions for the developed nonlinear model, the partial differential equation is converted to ordinary differential equation using the Galerkin’s decomposition procedure to decompose the spatial and temporal parts of the lateral displacement functions as

$$w(x,t)=\phi(x)q(t) \tag{29}$$

Where $u(t)$ the generalized coordinate of the system and $\phi(x)$ is a trial/comparison function that will satisfy both the geometric and natural boundary conditions.

Applying one-parameter Galerkin's solution given in Eq. (29) to Eq. (27)

$$\int_0^L R(x,t)\phi(x)dx \tag{30}$$

where

$$R(x,t)=(EI+E_sI_s)\frac{\partial^4 w}{\partial x^4}+(m_{cn}+m_f)\frac{\partial^2 w}{\partial t^2}+2m_f(1+a_kKn)\left[4\left(\frac{2-\sigma_v}{\sigma_v}\right)\left(\frac{Kn}{1+Kn}\right)+1\right]\frac{\partial^2 w}{\partial x\partial t}+\left[\frac{EA}{2L}\int_0^L\left(\frac{\partial w}{\partial x}\right)^2dx\right]\frac{\partial^2 w}{\partial x^2}$$

$$+\left(m_f\left[(1+a_kKn)\left[4\left(\frac{2-\sigma_v}{\sigma_v}\right)\left(\frac{Kn}{1+Kn}\right)+1\right]\right]^2+\delta A\sigma_x^o-H_s-\eta H_x^2A-k_p+\frac{EA\alpha\Delta T}{1-2\nu}\right)\frac{\partial^2 w}{\partial x^2}+k_1w+k_3w^3$$

$$-(e_oa)^2\left[\begin{array}{l}(m_{cn}+m_f)\dfrac{\partial^4 w}{\partial x^2\partial t^2}+2m_f(1+a_kKn)\left[4\left(\dfrac{2-\sigma_v}{\sigma_v}\right)\left(\dfrac{Kn}{1+Kn}\right)+1\right]\dfrac{\partial^4 w}{\partial x^3\partial t}+\left[\dfrac{EA}{2L}\displaystyle\int_0^L\left(\dfrac{\partial w}{\partial x}\right)^2dx\right]\dfrac{\partial^4 w}{\partial x^4}\\ +\left(m_f\left[(1+a_kKn)\left[4\left(\dfrac{2-\sigma_v}{\sigma_v}\right)\left(\dfrac{Kn}{1+Kn}\right)+1\right]\right]^2+\delta A\sigma_x^o-H_s-\eta H_x^2A-k_p+\dfrac{EA\alpha\Delta T}{1-2\nu}\right)\dfrac{\partial^4 w}{\partial x^4}\\ +k_1\dfrac{\partial^2 w}{\partial x^2}+3k_3w^2\dfrac{\partial^2 w}{\partial x^2}+6k_3w\left(\dfrac{\partial w}{\partial x}\right)^2\end{array}\right]=0$$

We have the nonlinear vibration equation of the pipe as

$$M\ddot{q}(t)+G\dot{q}(t)+(K+C)q(t)+Vq^3(t)=0 \tag{31}$$

where

$$M=(m_p+m_f)\left[\int_0^L\phi^2(x)dx-(e_oa)^2\int_0^L\phi^2(x)\frac{d^2\phi}{dx^2}dx\right]$$

$$G=\left[2m_f(1+a_kKn)\left[4\left(\frac{2-\sigma_v}{\sigma_v}\right)\left(\frac{Kn}{1+Kn}\right)+1\right]\right]\int_0^L\left[\phi(x)\left(\frac{d\phi}{dx}\right)dx-(e_oa)^2\int_0^L\phi(x)\frac{d^3\phi}{dx^3}dx\right]$$

$$K=\int_0^L(EI+E_sI_s)\phi(x)\frac{d^4\phi}{dx^4}dx+k_1\left[\int_0^L\phi^2(x)dx-(e_oa)^2\int_0^L\phi(x)\frac{d^2\phi}{dx^2}dx\right]$$

$$C=\left(\begin{array}{l}m_f\left[(1+a_kKn)\left[4\left(\dfrac{2-\sigma_v}{\sigma_v}\right)\left(\dfrac{Kn}{1+Kn}\right)+1\right]\right]^2\\ +\delta A\sigma_x^o-H_s-\eta H_x^2A-k_p+\dfrac{EA\alpha\Delta T}{1-2\nu}\end{array}\right)\left[\int_0^L\phi(x)\frac{d^2\phi}{dx^2}dx-(e_oa)^2\int_0^L\phi(x)\frac{d^4\phi}{dx^4}dx\right]$$

$$V=k_3\left[\int_0^L\phi^4(x)dx-(e_oa)^2\left(3\int_0^L\phi^3(x)\frac{d^2\phi}{dx^2}dx+6\int_0^L\phi^2(x)\left(\frac{d\phi}{dx}\right)^2dx\right)\right]$$

$$+\int_0^L\phi(x)\left[\frac{EA}{2L}\int_0^L\left(\frac{d\phi}{dx}\right)^2dx\right]\frac{d^2\phi}{dx^2}dx-(e_oa)^2\int_0^L\phi(x)\left[\frac{EA}{2L}\int_0^L\left(\frac{d\phi}{dx}\right)^2dx\right]\frac{d^4\phi}{dx^4}dx$$

The circular fundamental natural frequency gives

$$\omega_n=\sqrt{\frac{K+C}{M}} \tag{32}$$

For the simply supported pipe,

$$\phi(x) = sin\beta_n x \tag{33a}$$

where

$$sin\beta L = 0 \quad \Rightarrow \beta_n = \frac{n\pi}{L}$$

Therefore,

$$\phi(x) = sin\frac{n\pi x}{L} \tag{33b}$$

Eq. (33) can be written as

$$\ddot{q}(t) + \gamma_1\dot{q}(t) + \gamma_2 q(t) + \gamma_3 q^3(t) = 0 \tag{34}$$

where

$$\gamma_1 = \frac{(K+C)}{M}, \quad \gamma_3 = \frac{V}{M}, \quad \gamma_2 = \frac{G}{M},$$

For an undamped simple-simple supported structures, where *G = 0,* we have

$$\frac{d^2q(t)}{dt^2} + \gamma_1 q(t) + \gamma_3 q^3(t) = 0 \tag{35}$$

It can be seen from the above procedures that the apart from the fact that the Galerkin decomposition method decomposes governing equation of motion into spatial and temporal parts, it also helps in converting the space- and time-dependent partial differential equation to a time-dependent ordinary differential equation. The nonlinear ordinary differential equation easily be solved using numerical methods or approximate analytical methods. In this work, variational iteration method is adopted due to its simplicity and high level of accuracy.

4. Method of solution: Variational iteration method

In order to solve the nonlinear model in Eq. (35), variational iteration method is adopted in the present study. The basic definitions of the method are as follows:

The nonlinear differential equation in Eq. (35) can be written as

$$Lu + Nu = g(t) \tag{36}$$

where

L is a linear operator,

N is a nonlinear operator

g(t) is an inhomogeneous term in the differential equation.

Based on the VIM procedure, the correction functional can be written as

$$q_{n+1}(t) = q_n(t) + \int_0^t \lambda\left\{Lq_n(\tau) + N\tilde{q}(\tau) - g(t)\right\}d\tau \tag{37}$$

where

λ is a general Lagrange multiplier,

the subscript *n* is the nth approximation and $\tilde{q}$ is a restricted variation $\delta\tilde{q} = 0$

The correction functional in Eq. (37) is made stationary and also, considering $\delta u_{n+1} = 0$, gives

$$\delta q_{n+1}(t) = \delta q_n(t) + \lambda(\delta q_n)'\Big|_0^t - \lambda'(\delta q_n)'\Big|_0^t + \int_0^t \left\{\lambda'' + \lambda\gamma_1\right\}\delta q_n d\tau = 0 \tag{38}$$

Where its stationary conditions can be obtained as

$$\lambda''(\tau)+\omega^2\lambda(\tau)=0$$
$$\lambda(\tau)\big|_{\tau=t}=0 \tag{39}$$
$$1-\lambda'(\tau)\big|_{\tau=t}=0$$

The solution of Eq. (39), gives the Lagrange multiplier as

$$\lambda(\tau)=\frac{1}{\omega}sin\omega(\tau-t) \tag{40}$$

We can now write Eq. (40) as

$$q_{n+1}=q_n+\int_0^t\frac{1}{\omega}sin\omega(\tau-t)\left\{\left[\frac{d^2q_n(\tau)}{dt^2}+\omega^2q_n(\tau)\right]+\left[\gamma_1\tilde{q}_n(\tau)+\gamma_3\tilde{q}_n^3(\tau)-\omega^2\tilde{q}_n(\tau)\right]\right\}d\tau \tag{41}$$

The equations in the integral of Eq. (41) are grouped into linear and nonlinear parts based on the definition of VIM.

With the purpose of finding the periodic solution of Eq. (35), an initial approximation for zero-order deformation is assumed as

$$q_o(\tau)=Acos(\omega\tau) \tag{42}$$

Substituting Eq. (36) into the nonlinear part of Eq. (41), gives

$$N\left[q_0(\tau)\right]=\gamma_1cos(\omega\tau)+\gamma_3\left(Acos(\omega\tau)\right)^3-\omega^2Acos(\omega\tau) \tag{43}$$

After applying trigonometric identities, Eq. (43) can be written as

$$N\left[q_0(\tau)\right]=\gamma_1Acos(\omega\tau)+\gamma_3A^3\left(\frac{3cos(\omega\tau)+cos(3\omega\tau)}{4}\right)-\omega^2Acos(\omega\tau) \tag{44}$$

On collecting the like terms at the RHS of Eq. (44), one arrives at

$$N\left[q_0(\tau)\right]=\left(\gamma_1A-\omega^2A+\frac{3\gamma_3A^3}{4}\right)cos(\omega\tau)+\frac{\gamma_3A^3}{4}cos(3\omega\tau) \tag{45}$$

eliminate the secular term requires that the coefficient of $cos(\omega\tau)$ must be equal to zero. consequently,

$$\left(\gamma_1A-\omega^2A+\frac{3\gamma_3A^3}{4}\right)=0 \tag{46}$$

Therefore, the zero-order nonlinear natural frequency is given as

$$\omega_o\approx\sqrt{\gamma_1+\frac{3}{4}\gamma_3A^2} \tag{47}$$

Therefore, the ratio of the zero-order nonlinear natural frequency, ω_o to the linear frequency, ω_b

$$\frac{\omega_o}{\omega_b}\approx\sqrt{1+\frac{3}{4}\frac{\gamma_3A^2}{\gamma_1}} \tag{48}$$

where

$$\omega_b=\sqrt{\gamma_1}$$

Similarly, for the first-order nonlinear natural frequency, we have

$$\omega_1=\sqrt{\frac{1}{2}\left(\gamma_1+\frac{3\gamma_3A^2}{4}\right)+\sqrt{\left[\frac{1}{2}\left(\gamma_1+\frac{3\gamma_3A^2}{4}\right)\right]^2+\left(\frac{3\gamma_3^2A^4}{384}\right)}} \tag{49}$$

The ratio of the first-order nonlinear frequency, ω_l to the linear frequency, ω_b

$$\frac{\omega_1}{\omega_b} \approx \sqrt{\frac{1}{2}\left\{\left(1+\frac{3}{4}\frac{\gamma_3 A^2}{\gamma_1}\right)+\sqrt{\left(1+\frac{3}{4}\frac{\gamma_3 A^2}{\gamma_1}\right)^2+\left(\frac{3A^4}{384}\left(\frac{\gamma_3}{\gamma_1}\right)^2\right)}\right\}} \tag{50}$$

From Eqs. (48) and (50), the following facts are established:

$$\lim_{A\to 0}\frac{\omega}{\omega_b}=1 \tag{51}$$

and

$$\lim_{A\to \infty}\frac{\omega}{\omega_b}=\infty \tag{52}$$

In order to find the first iteration, we can write Eq. (41) as

$$q_1 = q_0 + \int_0^t \frac{1}{\omega} sin\omega(\tau - t)\left\{\left[\frac{d^2 q_0(\tau)}{dt^2}+\omega^2 q_0(\tau)\right]+\left[\gamma_1\tilde{q}_0(\tau)+\gamma_3\tilde{q}_0^3(\tau)-\omega^2\tilde{q}_0(\tau)\right]\right\}d\tau \tag{53}$$

Substituting Eqs. (42) into Eq. (53), we have

$$q_1 = q_0 + \int_0^t \frac{1}{\omega} sin\omega(\tau - t)\left\{\left[-A\omega^2 cos(\omega\tau)+\omega^2 Acos(\omega\tau)\right]+\left[\begin{array}{l}\gamma_1 Acos(\omega\tau)+\gamma_3\left(Acos(\omega\tau)\right)^3\\ -\omega^2 Acos(\omega\tau)\end{array}\right]\right\}d\tau \tag{54}$$

Which reduces to

$$q_1 = q_0 + \int_0^t \frac{1}{\omega} sin\omega(\tau - t)\left\{-A\omega^2 cos(\omega\tau)+\gamma_1 Acos(\omega\tau)+\gamma_3\left(Acos(\omega\tau)\right)^3\right\}d\tau \tag{55}$$

With the aids of trigonometric identities, Eq. (55) can be written as

$$q_1 = q_0 + \int_0^t \frac{1}{\omega} sin\omega(\tau - t)\left\{-A\omega^2 cos(\omega\tau)+\gamma_1 Acos(\omega\tau)+\gamma_3 A^3\left(\frac{3cos(\omega\tau)+cos(3\omega\tau)}{4}\right)\right\}d\tau \tag{56}$$

Evaluation of the above Eq. (56) provides the first-order approximation as

$$q_1(t)=\left(A-\frac{\gamma_3 A^3}{32\omega^2}\right)cos(\omega t)+\frac{\gamma_3 A^3}{32\omega^2}cos(3\omega t)+tA\left(\frac{\omega}{2}-\frac{3\gamma_3 A^2}{8\omega}-\frac{\gamma_1}{2\omega}\right)sin(\omega t) \tag{57}$$

Eq. (57) can be written as

$$q(t)\approx A\left\{\left(1-\frac{\gamma_3 A^2}{32\omega^2}\right)cos(\omega t)+\frac{\gamma_3 A^2}{32\omega^2}cos(3\omega t)+t\left(\frac{\omega}{2}-\frac{3\gamma_3 A^2}{8\omega}-\frac{\gamma_1}{2\omega}\right)sin(\omega t)\right\} \tag{58}$$

From Eqs. (29) and (33b), one has

$$w(x,t)\approx A\left\{\left(1-\frac{\gamma_3 A^2}{32\omega^2}\right)cos(\omega t)+\frac{\gamma_3 A^2}{32\omega^2}cos(3\omega t)+t\left(\frac{\omega}{2}-\frac{3\gamma_3 A^2}{8\omega}-\frac{\gamma_1}{2\omega}\right)sin(\omega t)\right\}sin\left(\frac{\beta x}{L}\right) \tag{59}$$

where

$$\omega_1 = \sqrt{\frac{1}{2}\left(\gamma_1+\frac{3\gamma_3 A^2}{4}\right)+\sqrt{\left[\frac{1}{2}\left(\gamma_1+\frac{3\gamma_3 A^2}{4}\right)\right]^2+\left(\frac{3\gamma_3^2 A^4}{384}\right)}}$$

Therefore,

$$w(x,t)\approx A\left\{\begin{aligned}&\left(1-\frac{\gamma_3A^2}{32\left(\frac{1}{2}\left(\gamma_1+\frac{3\gamma_3A^2}{4}\right)+\sqrt{\left[\frac{1}{2}\left(\gamma_1+\frac{3\gamma_3A^2}{4}\right)\right]^2+\left(\frac{3\gamma_3^2A^4}{384}\right)}\right)}\right)cos\left(\sqrt{\frac{1}{2}\left(\gamma_1+\frac{3\gamma_3A^2}{4}\right)+\sqrt{\left[\frac{1}{2}\left(\gamma_1+\frac{3\gamma_3A^2}{4}\right)\right]^2+\left(\frac{3\gamma_3^2A^4}{384}\right)}}\right)t\\&+\frac{\gamma_3A^2}{32\left(\frac{1}{2}\left(\gamma_1+\frac{3\gamma_3A^2}{4}\right)+\sqrt{\left[\frac{1}{2}\left(\gamma_1+\frac{3\gamma_3A^2}{4}\right)\right]^2+\left(\frac{3\gamma_3^2A^4}{384}\right)}\right)}cos\left(3\sqrt{\frac{1}{2}\left(\gamma_1+\frac{3\gamma_3A^2}{4}\right)+\sqrt{\left[\frac{1}{2}\left(\gamma_1+\frac{3\gamma_3A^2}{4}\right)\right]^2+\left(\frac{3\gamma_3^2A^4}{384}\right)}}\right)t\\&+t\left(\begin{aligned}&\frac{\left(\sqrt{\frac{1}{2}\left(\gamma_1+\frac{3\gamma_3A^2}{4}\right)+\sqrt{\left[\frac{1}{2}\left(\gamma_1+\frac{3\gamma_3A^2}{4}\right)\right]^2+\left(\frac{3\gamma_3^2A^4}{384}\right)}}\right)}{2}\\&-\frac{3\gamma_3A^2}{8\left(\sqrt{\frac{1}{2}\left(\gamma_1+\frac{3\gamma_3A^2}{4}\right)+\sqrt{\left[\frac{1}{2}\left(\gamma_1+\frac{3\gamma_3A^2}{4}\right)\right]^2+\left(\frac{3\gamma_3^2A^4}{384}\right)}}\right)}\\&-\frac{\gamma_1}{2\left(\sqrt{\frac{1}{2}\left(\gamma_1+\frac{3\gamma_3A^2}{4}\right)+\sqrt{\left[\frac{1}{2}\left(\gamma_1+\frac{3\gamma_3A^2}{4}\right)\right]^2+\left(\frac{3\gamma_3^2A^4}{384}\right)}}\right)}\end{aligned}\right)sin\left(\sqrt{\frac{1}{2}\left(\gamma_1+\frac{3\gamma_3A^2}{4}\right)+\sqrt{\left[\frac{1}{2}\left(\gamma_1+\frac{3\gamma_3A^2}{4}\right)\right]^2+\left(\frac{3\gamma_3^2A^4}{384}\right)}}\right)t\end{aligned}\right\}sin\left(\frac{\beta x}{L}\right) \tag{60}$$

4. Results and Discussion

With the aid of MATLAB, the results of the simulations are given in Figs. 3-12. While Fig. 3 presents the comparison of the results of the present study with results of numerical solution using finite difference method, the effects of various parameters of the model on the dynamic response of the single-walled carbon nanotube are also presented in the figures under various subsections in the section in Figs. 4-14.

Fig. 4 illustrates the importance of surface residual stress on the vibration behaviour of the nanotube. It is shown that the dynamic response of the nanotube different for negative and positive values of surface residual stress. This establishes that the dynamic behaviour of the fluid-conveying nanotube depends on the sign of the residual surface stress. Indisputably, as it is shown in the figure, at any given adimensional amplitude, there is an increase in the frequency ratio when the negative value of the surface stress increases while the frequency ratio decreases when the positive value of the surface stress increases. This is because, the negative values of surface stress decrease the linear stiffness of the nanostructure while the positive values of surface stress increase the linear stiffness of the carbon nanotube. Also, considering the effect of surface stress, the positive surface elasticity produces softening effect in the nanotube, while negative surface elasticity gives stiffening influence in the nanotube. Therefore, it can be stated that when the surface stress is zero, the effect of surface elasticity is not so important. Consequently, one can infer that the surface stress alone is important and effective even without consideration of the surface elasticity. However, when the surface stress is nonzero, the surface elasticity plays a significant role in the dynamic behaviour of the nanostructure.

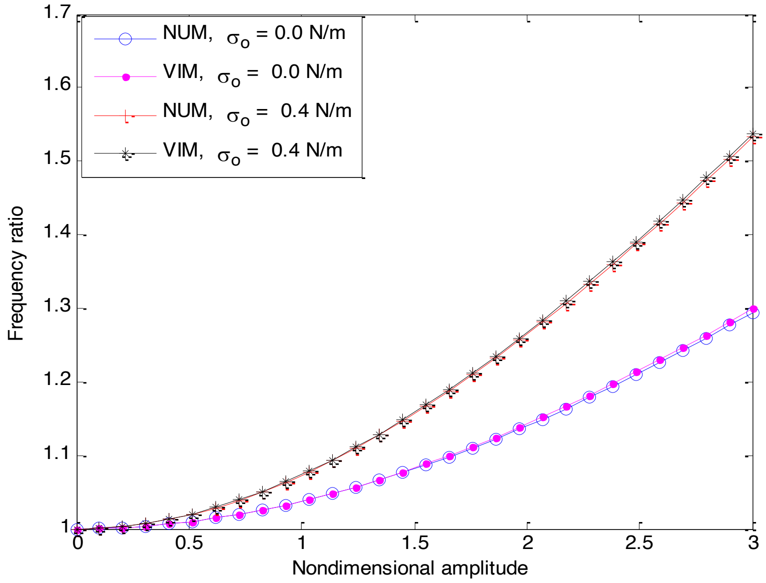

Fig. 3 Comparison between the obtained results and the numerical solution for the nonlinear vibration

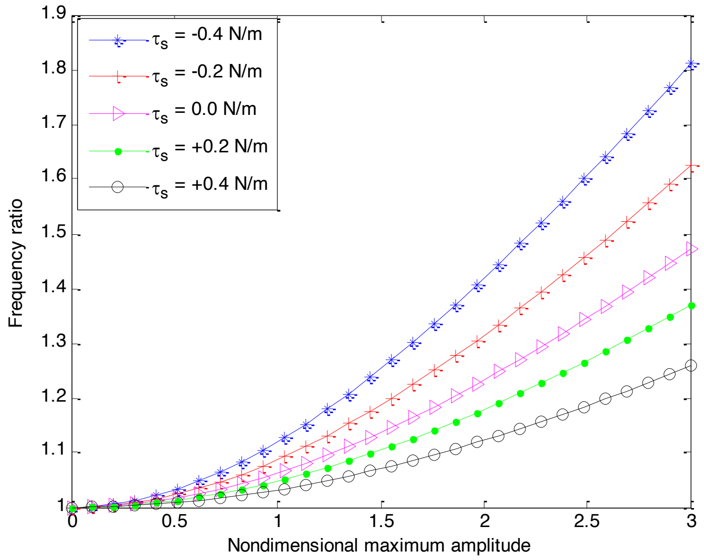

Fig. 4 Effect of surface residual stress per unit length on the frequency ratio of the nanotube

Fig. 5 displays the significance of surface stress, nonlocality and nanobeam length on the frequency ratio of the fluid-conveying nanostructure. The figures show that the frequency ratio decreases with increase in the length and thickness ratio of the of the nanotube. It could also be stated that nonlocal parameter reduces the influence of the surface energy and stress on the frequency ratio. The results also presented that the vibration frequency of the nanotube under the consideration of the effects of surface energy and stress is larger than vibration frequency of the nanobeam given by the classical beam theory which does not consider the surface effect. Also, the figures present a clear statement that when the nanotube length increase, the natural frequency of the nanotube gradually approaches the nonlinear Euler–Bernoulli beam limit. This is as a result of decrease in the surface effect. Therefore, high thickness ratios and long nanotube length make the impacts of surface energy and stresses on the on the frequency ratio to vanish. **Fig. 6** shows the effect of initial stress on the dynamic behaviour of the nanotube. It is depicted at any adimensional amplitude increases, there is an increase in the frequency ratio as the initial stress increases.

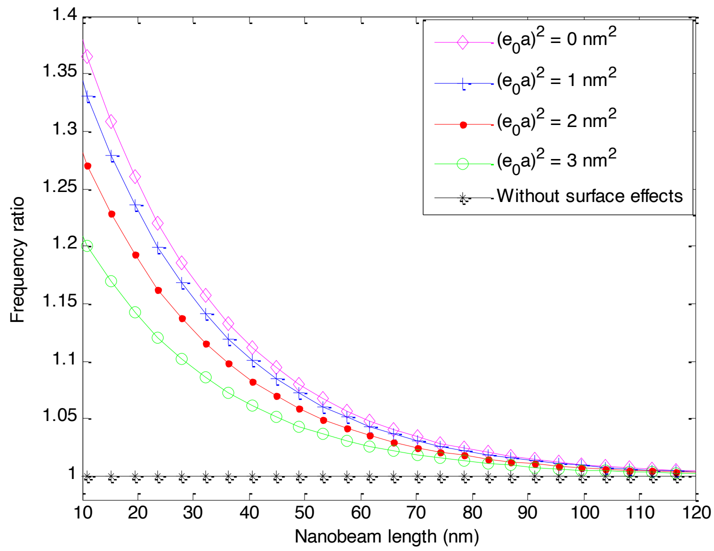

Fig. 5 Effects of the nanotube nonlocal parameter and length on the frequency ratio

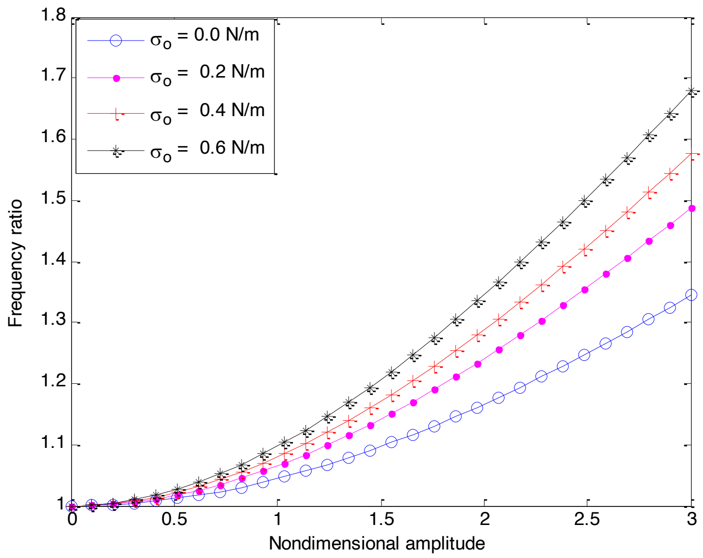

Fig. 6 Effect of initial stress on the frequency ratio of the nanotube

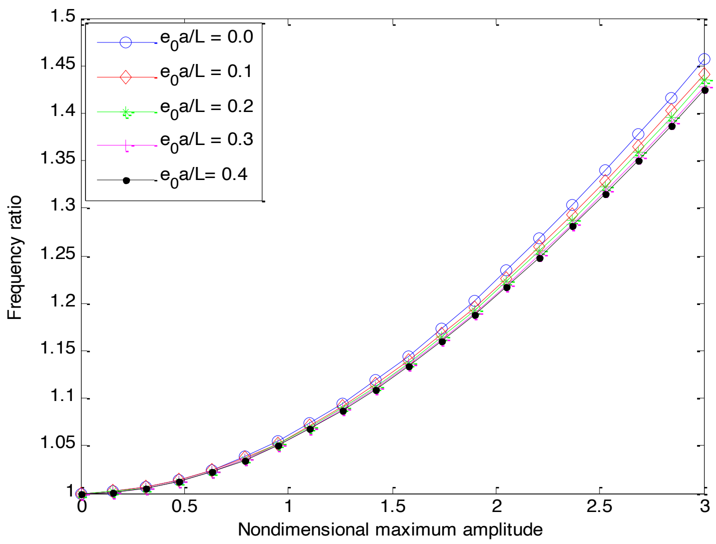

Fig. 7 Effects of maximum amplitude and nonlocal parameter on ratio of the frequency ratio

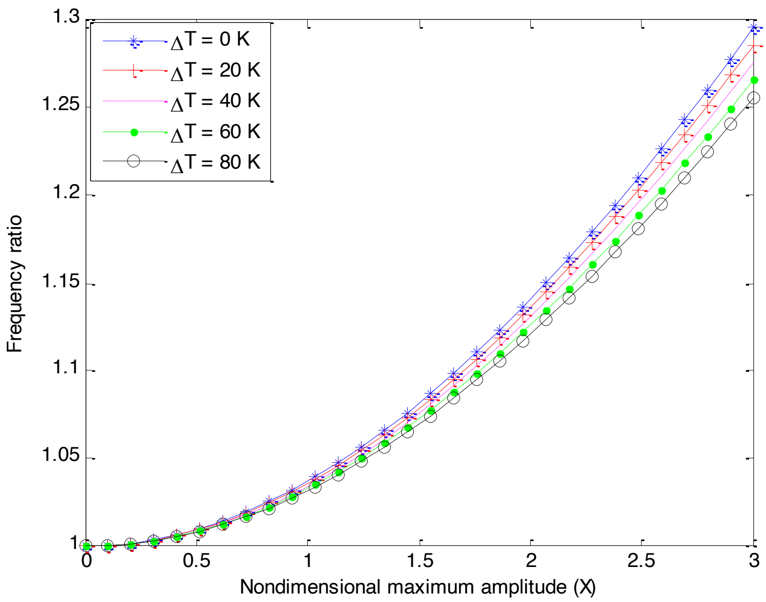

Fig. 8 Effects of change in temperature on the frequency at high temperature

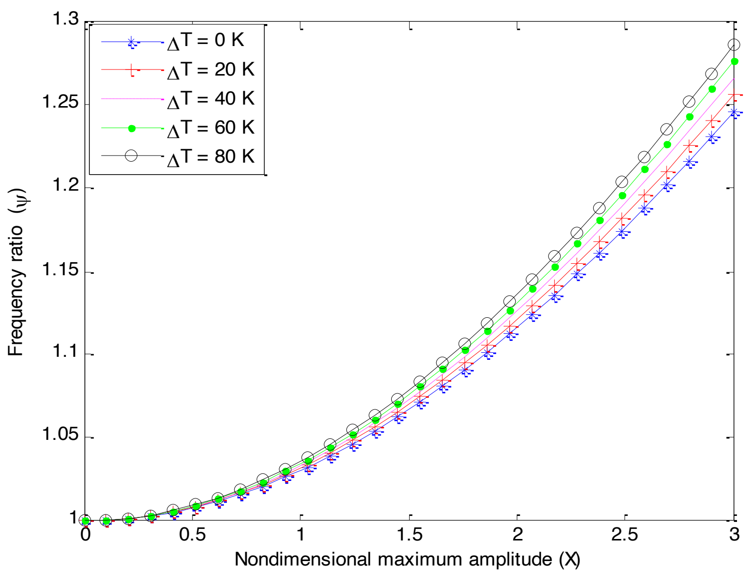

Fig. 9 Effects of change in temperature on the frequency ratio at low temperature

The nonlocal parameter is a scaling parameter which makes the small-scale effect to be accounted in the analysis of microstructures and nanostructures. Fig 7 depicts the effect of the nonlocality on the frequency ratio decrease for varying adimensional amplitude. The fundamental frequency ratio of the fluid-conveying structure decreases as the nonlocal parameter increases. Also, the effect of the nonlocality on the frequency ratio decreases by increasing the amplitude ratio of the structure.

The variations in the ratio of the frequencies with adimensional nonlocal parameter for different change in temperature are presented in Figs. 8 and 9. In Fig. 8, it is shown that increase in temperature change at high temperature causes decrease in the frequency ratio. However, at room or low temperature, the frequency ratio of the hybrid nanostructure increases as the temperature change increases as shown in Fig. 8. Also, the ratio of the frequencies at low temperatures is lower than at high temperatures.

The effect of magnetic field strength on the frequency ratio of the nanotube is shown in Fig. 10. It is shown that the frequency ratio decreases when the strength of the magnetic field increases. Also, at high values of magnetic fields and amplitude of vibration, the discrepancy between the nonlinear and the linear frequencies increases. A further investigation shows that the vibration of the nanotube approaches linear vibration when the magnetic force strength increases to a certain high value. Such very high value of magnetic force strength which causes great attenuation in the beam can be adopted as a control and instability strategy for the nonlinear vibration system.

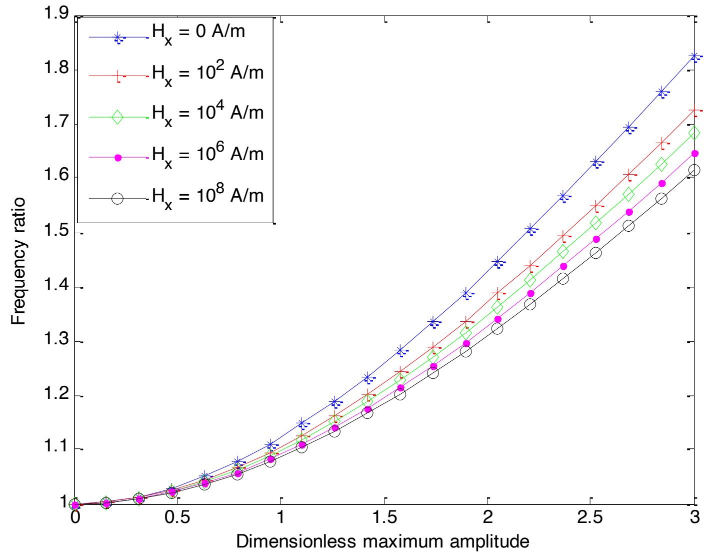

Fig. 10 Effects of magnetic field strength on the frequency ratio

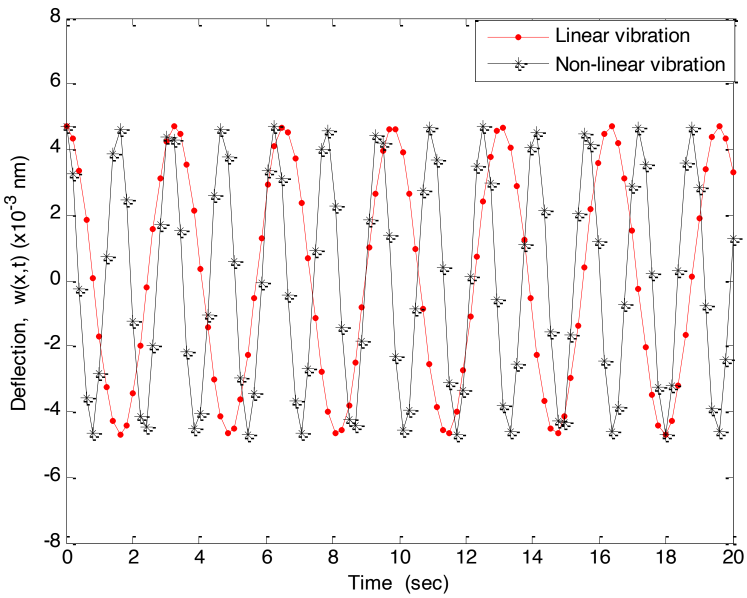

Fig. 11 Linear and nonlinear dynamic behaviour of the nanostructure

Fig. 11 shows the comparison of the midpoint deflection of linear and nonlinear vibrations of the nanostructure. The nonlinear term causes stretching effect in the nonlinear in the nonlinear vibration. As stretching effect increases, the stiffness of the system increases which consequently increases in the natural frequency and the critical fluid velocity. Effects of nonlocal and slip parameters on the vibration of the nanotube is shown in Figs 12-14. It is depicted that increase in the nonlocal and slip parameters leads to decrease in the frequency of vibration and decrease in the critical velocity. Also, the Figures. depict the critical speeds corresponding to the divergence condition for different values of the system's parameters for the varying nonlocal and slip parameters.

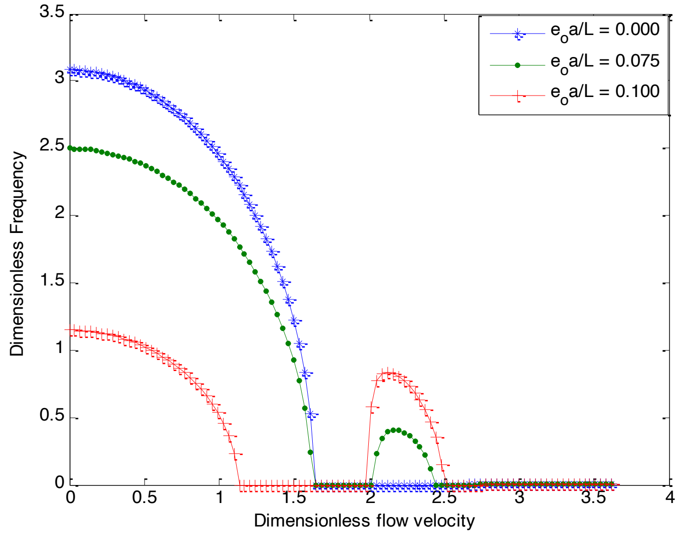

Fig. 12 Effects of nonlocal parameter and fluid flow velocity on the natural frequency of the nonlinear vibration

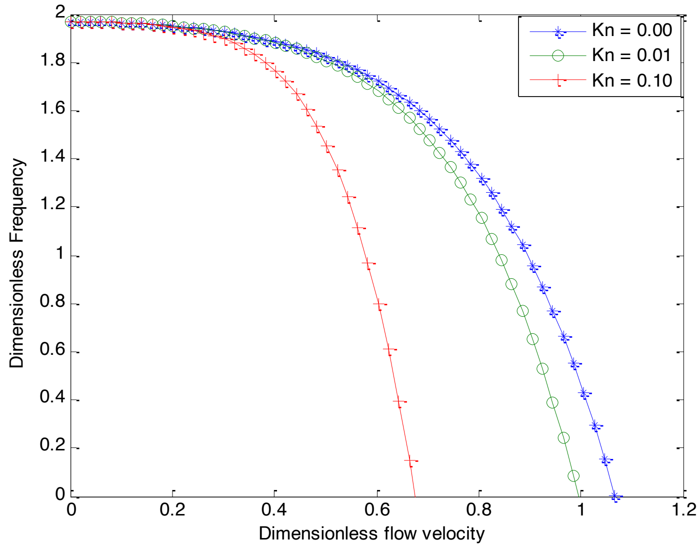

Fig. 13 Effects Slip parameter (Knudsen number) on the natural frequency of the nonlinear vibration

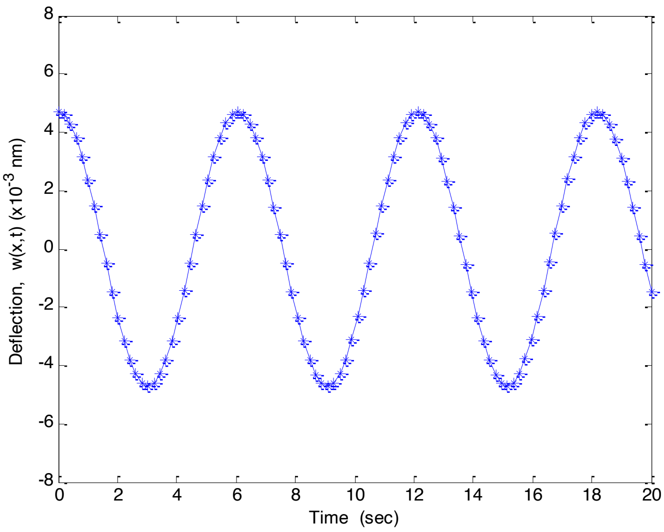

Fig. 14a Effects of slip parameter on the deflection of the nonlinear vibration when Kn=0.03

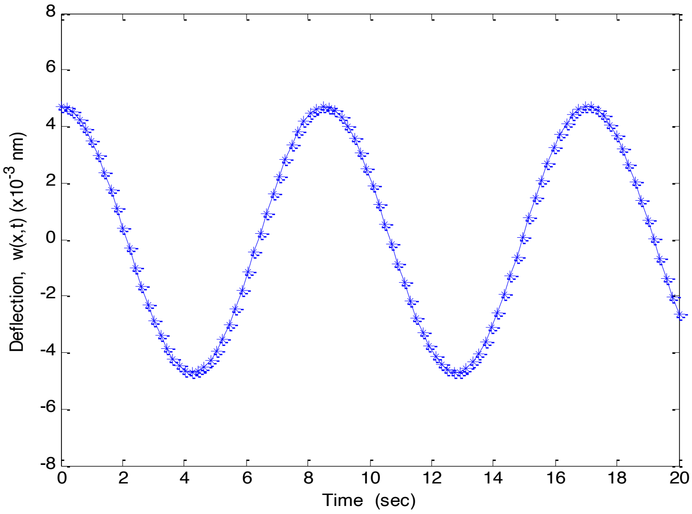

Fig. 14b Effects of slip parameter on the deflection of the nonlinear vibration when Kn = 0.05

Conclusion

In the current paper, the simultaneous impacts of surface elasticity, initial stress, residual surface tension and nonlocality on the nonlinear vibration of single-walled carbon conveying nanotube resting on linear and nonlinear elastic foundation and operating in a thermo-magnetic environment have been analyzed using variational iterative method. Through the parametric studies, it was revealed that the

i. ratio of the nonlinear to linear frequencies increases with the negative value of the surface stress while it decreases with the positive value of the surface stress. At any given value of nonlocal parameters, the surface effect reduces for increasing in the length of the nanotube.
ii. ratio of the frequencies decreases with increase in the strength of the magnetic field, nonlocal parameter and the length of the nanotube. The natural frequency of the nanotube gradually approaches the nonlinear Euler–Bernoulli beam limit at high values of nonlocal parameter and nanotube length.
iii. nonlocal parameter reduces the surface effects on the ratio of the frequencies.
iv. increase in temperature change at high temperature causes decrease in the frequency ratio. However, at room or low temperature, the frequency ratio of the hybrid nanostructure increases as the temperature change increases. Also, the ratio of the frequencies at low temperatures is lower than at high temperatures.
v. increase in the nonlocal and slip parameters leads to decrease in the frequency of vibration and decrease in the critical velocity.

The present work will assist in the control and design of carbon nanotubes operating in thermo-magnetic environment and resting on elastic foundations.

Nomenclature

A	Area of the nanotube	T	change in temperature.
E	Modulus of Elasticity	t	time coordinate
EI	bending rigidity	w	transverse displacement/deflection of the nanotube
H_s	residual surface stress	W	time-dependent parameter
H_x	magnetic field strength	x	axial coordinate
I	moment of area	$\phi(x)$	trial/comparison function
L	length of the nanotube	α_x	coefficient of thermal expansion
m_c	mass of tube per unit length	η	magnetic field permeability
N	axial/Longitudinal force		

References

Abgrall P. and Nguyen N. T. (2008). Nanofluidic devices and their applications," *Anal. Chem.,* 80, 2326–2341. Zhao D., Liu Y. and Tang Y. G. (2018). Effects of magnetic field on size sensitivity of nonlinear vibration of embedded nanobeams,"Mech. *Adv. Mater. Struct.,*1–9.

Arania A. G., Roudbaria M. A., Amir S. (2016). Longitudinal magnetic field effect on wave propagation of fluid conveyed SWCNT using Knudsen number and surface considerations. *Applied Mathematical Modelling 40*, 2025–2038.

Azrar A., Ben Said M., Azrar L. and Aljinaidi A. A. (2018). Dynamic analysis of Carbon Nanotubes conveying fluid with uncertain parameters and random excitation," *Mech. Adv. Mater. Struct*., 1–16. Rashidi, V., Mirdamadi, H. R. and Shirani, E. (2012). A novel model for vibrations of nanotubes conveying nanoflow. *Comput. Mater. Sci*., 51, 347–352.

Bahaadini R. and Hosseini (2016). Effects of nonlocal elasticity and slip condition on vibration and stability analysis of viscoelastic cantilever carbon nanotubes conveying fluid," *Comput. Mater. Sci*., 114, 151–159, 2016.

Bahaadini R. and Hosseini (2016). Nonlocal divergence and flutter instability analysis of embedded fluid-conveying carbon nanotube under magnetic field," *Microfluid. Nanofluid*., 20, 108.

Bahaadini R. and Hosseini (2018). Flow-induced and mechanical stability of cantilever carbon nanotubes subjected to an axial compressive load," *Appl. Math. Modelling*., 59, 597–613.

Bahaadini R. and Hosseini, Jamalpoor A. (2017). Nonlocal and surface effects on the flutter instability of cantilevered nanotubes conveying fluid subjected to follower forces," *Physica B*., 509, 55–61.

Chen X. and Wang X. (2008). Effects of initial stress on wave propagation in multi-walled carbon nanotubes *Phys. Scr*. 78, 015601 (9pp).

Eringen A.C. (1972). Linear theory of nonlocal elasticity and dispersion of plane waves*. Int. J. Eng. Sci*. 10(5), 425–435.

Eringen A.C. (1983). On differential equations of nonlocal elasticity and solutions of screw dislocation and surface waves. *J. Appl. Phys*. 54(9), 4703–4710.

Eringen A.C. (1972). Nonlocal polar elastic continua. *Int. J. Eng. Sci*. 10(1), 1–16 (1972)

Farshi B, Assadi A, Alinia-ziazi A. (2010). Frequency analysis of nanotubes with consideration of surface effects. *Appl Phys Lett.* 96:093103–5.

Feng X. Q, Xia R, Li X. D, Li B. (2009). Surface effects on the elastic modulus of nanoporous materials. *Appl Phys Lett* 94:011913–6.

Guo J. G. (2007), Zhao Y. P. The size-dependent bending elastic properties of nanobeams with surface effects. *Nanotechnology*.18:295701–6.

He J, Lilley C. M. (2008). Surface stress effect on bending resonance of nanowires with different boundary conditions. *Appl Phys Lett*. 93, 263103–8.

He J. Lilley C. M. (2008). Surface effect on the elastic behavior of static bending nanowires. *Nano Lett*. 8:1798–802.

Hosseini M., Bahaadini R. and B. Jamali B. (2016). Nonlocal instability of cantilever piezoelectric carbon nanotubes by considering surface effects subjected to axial flow," *J. Vib. Control* .24(9).

Iijima S. (1991), Helical microtubules of graphitic carbon. *Nature*, 354, 56–58.

Jing G. Y., Duan H. L., Sun X. M., Zhang Z. S., Xu J, Li Y.D., et al. (2006). Surface effects on elastic properties of silver nanowires: contact atomic-force microscopy. *Phys. Rev. B*. 73, 235406–9; https://doi.org/10.1103/PhysRevB.73.235409

Lee H. L, Chang W. J. (2011). Surface effects on axial buckling of non-uniform nanowires using non-local elasticity theory. *Micro & Nano Letters*, IET, 6(1), 19-21.

Lee H. L. Chang W. J. (2010). Surface effects on frequency analysis of nanotubes using nonlocal Timoshenko beam theory. *J Appl Phys*. 108, 093503-3.

Lim C. W. and Yang Y. (2010). New predictions of size-dependent nanoscale based on nonlocal elasticity for wave propagation in carbon nan- otubes," *J. Comput. Theor. Nanoscience*., 7, 988–995.

Lim C. W. (2010). On the truth of nanoscale for nanobeams based on nonlocal elastic stress field theory: equilibrium, governing equation and static deflection. *Appl. Math. Mech*., 31, 37–54.

Sun C. and Liu K. (2007). Vibration of multi-walled carbon nanotubes with initial axial loading , *Solid State Communications* 143, 202–207. https://doi.org/10.1016/j.ssc.2007.05.027

Mahinzare M., Mohammadi K. Ghadiri M. and Rajabpour A. (2017). Size-dependent effects on critical flow velocity of a SWCNT conveying viscous fluid based on nonlocal strain gradient cylindrical shell model," *Microfluid. Nanofluid*, 21, 123.

Reddy J. N. and Pang S. (2008). Nonlocal continuum theories of beams for the analysis of carbon nanotubes," *J. Appl. Phys*., 103, 023511.

Selim M. M. (2011) Vibrational analysis of initially stressed carbon nanotubes. *Acta Phys Pol A*.119(6), 778–82

Selim M. M. (2009). Vibrational analysis of carbon nanotubes under initial compression stresses , *NANO Conference*, April 5-7, 2009, King Saud University, KSA.

Selim M. M. and El-Safty S.A. (2020) Vibrational analysis of an irregular single-walled carbon nanotube incorporating initial stress effects. *Nanotechnology Reviews*; 9, 1481–1490

Selim M. M. (2010). Torsional vibration of carbon nanotubes under initial compression stress. *Brazilian Journal of Physics*, 40(3), 283-287, https://doi.org/10.1590/S0103-97332010000300004

Selim M. M. (2011). Vibrational Analysis of Initially Stressed Carbon Nanotubes. *Acta Physica Polonica A*, 119.

Sharm P, Ganti S., Bhate N. (2003). Effect of surfaces on the size-dependent elastic state of nano-inhomogeneities. *Appl. Phys. Lett.* 82, 535–7.

Wang G. F. Feng X. Q. (2009). Surface effects on buckling of nanowires under uniaxial compression. *Appl Phys Lett*. 94, 141913-3.

Wang G. F., Feng X. Q. (2007). Effects of surface elasticity and residual surface tension on the natural frequency of micro-beams. *Journal of Applied Physics*, 101, 013510.

Wang H. and Cai H. (2006). Effects of initial stress on non-coaxial resonance of multi-wall carbon nanotubes, *Acta Mater*. 54, 2067–2074.

Wang L. (2010). Vibration analysis of fluid-conveying nanotubes with con-sideration of surface effects," *Physica E*., 43, 437–439.

Wang L. (2011). A modified nonlocal beam model for vibration and stability of nanotubes conveying fluid," *Physica E*., 44, 25–28, 2011.

Wang Z. Q, Zhao Y. P, Huang Z. P. (2010). The effects of surface tension on the elastic properties of nano structures. *Int J Eng Sci*. 48:140–50.

Zhang H. and Wang X. (2006). Effects of initial stress on transverse wave propagation in carbon nanotubes based on Timoshenko laminated beam models, *Nanotechnoology* 17, 45-53.

Zhang J. and Meguid S. A. (2016). Effect of surface energy on the dynamic response and instability of fluid-conveying nanobeams. *Eur. J. Mech. – A / Solids*., 58, 1–9. https://doi.org/10.1016/j.euromechsol.2016.01.001